JOURNAL OF MATERIALS SCIENCE **39** (2004) 3619– 3628

Fibre orientation effects on the fracture of short fibre polymer composites: on the existence of a critical fibre orientation on varying internal material variables

S. FARA, A. PAVAN
Dipartimento di Chimica, Materiali e Ingegneria Chimica "Giulio Natta," Politecnico di Milano, Piazza Leonardo da Vinci 32, I-20133 Milano, Italy
E-mail: andrea.pavan@polimi.it

The dependence of fracture toughness on fibre orientation, in short fibre reinforced polymers, was investigated using materials with different polymer matrix (polyamide 6.6, polyarylamide and polyoxymethylene), fibre sizing, fibre content, mean fibre length and fibre length distribution.

To assess the dependence on fibre orientation, plates with unidirectionally oriented fibres were prepared and cut at various angles with respect to the direction of the aligned fibres. The fracture behaviour was investigated by single-edge notch three-point bending tests. In addition the stress-strain behaviour was examined by performing uniaxial tension and compression tests.

Both the critical stress intensity factor K_C and the fracture energy G_C measured at fracture initiation were found to present a bi-linear relationship to the factor characterizing fibre orientation, with different slopes over different ranges of the orientation factor. This suggested the occurrence of a transition between different failure mechanisms with varying fibre orientation, namely matrix fracture and fibre debonding at low values of the fibre orientation factor, fibre breakage and pull-out at high values of the fibre orientation factor. This interpretation is supported by the observation of the crack growth direction (which varies with varying fibre orientation) and the analysis of the fracture surfaces. The slopes of the two linear branches of the toughness vs. fibre-orientation-factor plot and the "critical" fibre orientation angle depend on all internal variables investigated: constituent polymer matrix, degree of fibre-matrix adhesion, fibre content, mean fibre length and fibre length distribution.

List of symbols

a_0	notch depth (mm)
a_{ij}^0	components of the Advani-Tucker tensor or fibre orientation factor to respect the reference system $1^0 2^0 3^0$
a_{ij}	components of the Advani-Tucker tensor or fibre orientation factor to respect the reference system 123
$(a_{11})_C$	critical fibre orientation factor a_1
B	plate and specimen thickness (mm)
d	fibre diameter (μm)
E	Young's modulus (GPa)
E_{ii}	Young's modulus (GPa) in the principal directions (where *1* is the nominal fibre direction)
F_k	weighting factor of the k-th fibre (μm^{-1})
$f_{p,eff}$	effective orientation factor
G_C	fracture energy (kJ m^{-2})
G_{ij}	shear modulus (GPa) in the principal directions (where *1* is the nominal fibre direction)
H	prismatic specimen height (mm)
K_C	critical stress intensity factor (MPa $m^{1/2}$)
l	fibre length (μm)
l_C	critical fibre length (μm)
l_K	length of the k-th fibre (μm)
l_m	mass average fibre length (μm)
l_n	number average fibre length (μm)
n	normal to section
$\vec{p}$	unit vector
p_i^0	component of the unit vector $\vec{p}$ aligned with the k-th fibre with respect to axes i^0
p_i	component of the unit vector $\vec{p}$ aligned with the k-th fibre with respect to axes i
R	reinforcing effectiveness parameter
S	fracture specimen span (mm)
v_f	fibre volume fraction or percent (%)

W	fracture specimen width (mm)
w_f	fibre weight percent (%)
α	angle between the applied stress direction and the extruded rods or mould fill direction
ε	axial strain
θ_k	angle between the k-th fibre and the normal to section plane
ν_{ij}	Poisson's ratio in the principal directions (where *1* is the nominal fibre direction)
ρ	axial stress (MPa)
σ_f	fibre tensile strength (MPa)
σ^u	failure axial stress (MPa)
σ^u_{ii}	failure axial stress (MPa) in the principal directions (where *1* is the nominal fibre direction)
τ_i	fibre-matrix adhesion (MPa)
τ^u_{ij}	failure shear stress (MPa) in the principal directions (where *1* is the nominal fibre direction)

1. Introduction

Short fibre polymer composites are attractive structural materials for their relatively easy processability, e.g., by conventional injection moulding. When a processing technique such as this is used, however, a complex microstructure may result, with different fibre orientations at different points of the moulded piece, depending on the resultant flow field and cooling conditions. Since the local mechanical properties of the material are strongly governed by its microstructure, the overall properties of these structured materials cannot be described without specifying their microstructural characteristics. As a consequence, their prediction is a complex but industrially crucial problem with these materials.

The dependence of stiffness, strength and fracture toughness on some characteristics of the constituent fibres such as fibre volume fraction and fibre length has been investigated for long time. It is well known that a critical fibre length l_C exists, and separates two different fracture mechanisms [1]: fibre pull-out is the prevailing fracture mechanism when fibre length is shorter than the critical fibre length ($l < l_C$), whereas fibre breakage occurs when fibre length is larger than the critical one ($l > l_C$).

By contrast, the influence of fibre orientation has not often been properly considered. A thorough fibre orientation characterisation of these materials is seldom performed, perhaps because the analytical technique required is cumbersome and time consuming. Some authors do not even care to make any fibre orientation determination at all, others make just a gross structural characterisation, often based only on macroscopic observations (e.g., by examination of the fracture surface). So, the structure of an injection moulded plate is often described as a three-layer laminate with two outer skin layers having fibres predominantly aligned to the mould fill direction, and a core layer with fibres predominantly oriented in the transverse direction. This kind of structure is described in terms of the thicknesses of the layers, or of their ratio and the properties of the material, such as the fracture toughness, are then tentatively correlated to this parameter [2, 3].

The need for a more detailed microstructural characterisation of short fibre composite materials in relation to fracture toughness, including fibre orientation and its distribution along the crack front, was pointed out by Friedrich [4] and Friedrich *et al*. [5, 6]. They assumed that fracture toughness is linearly dependent on a reinforcing effectiveness parameter, R, which is directly related to the geometrical characteristics of the fibres and their special arrangement through the plate thickness. The relationship between R and the fibre spatial arrangement is expressed through an "effective fibre orientation parameter" arbitrarily assumed.

More recently, however, other authors [7, 8] have questioned this latter assumption and have underlined the need of relating fracture toughness and crack hindrance effects of the fibres to their orientation more accurately, on the basis of the observation that different failure mechanisms may occur with different fibre orientations, as shown experimentally in [9].

We have thus undertaken an extensive experimental programme aimed at investigating the dependence of fracture toughness on fibre orientation over a wide range of material systems (different internal variables) and testing conditions (different external variables) [10].

In this work we start considering the simplest case of unidirectional short fibre composites and examine a number of internal variables (namely polymer matrix, fibre sizing, fibre content, mean fibre length and fibre length distribution) under equal testing conditions.

To assess the dependence on fibre orientation plates with unidirectionally oriented fibres were prepared and cut and tested at various angles with respect to the direction of the aligned fibres. Fibre orientation was checked by computer image analysis of plane sections of the plates observed under an optical microscope and described in terms of the Advani-Tucker tensor components [11]. The fracture behaviour was investigated by single-edge notch three-point bending tests, and two variant of fracture toughness, i.e., the critical stress intensity factor K_C and the fracture energy G_C, were determined at fracture initiation. Finally, the crack growth direction was observed under an optical microscope and the fractured specimen surfaces were examined using a scanning electron microscope to assess the fracture mechanisms involved.

In addition, the stress-strain behaviour of all materials was examined as a function of fibre orientation by performing uniaxial tension and compression tests at varying angle with respect to the fibre direction.

2. Experimental

2.1. Materials

Different supplies of short glass fibre reinforced polymers were used for the experimental programme considered in the present work.

Two samples of polyamide 6.6 (PA66) containing 30 wt% of glass fibre (G30) with two different fibre surface treatments (here denoted A and B) were provided in the form of thin extruded rods (~2–3 mm in diameter) by Radici NovaCips, Villa D'Ogna, Italy. Two samples of polyoxymethylene (POM) with a different content of glass fibre, i.e., 15 and 30 wt% (G15 and G30), were provided in the form of thin extruded rods

(∼1–2 mm in diameter) by Rhodia, Ceriano Laghetto, Italy. The orientation of the fibres in these rods was found to be highly unidirectional thus offering the possibility of preparing plates with unidirectional fibre orientation by a technique consisting in aligning, adjoining, compacting, and remoulding several of these rods in a hot press mould [7]. To this end the rods were first kiln dried at 80°C for 90 h in the case of PA66 and at 80°C for 16 h in the case of POM and then compression moulded at 290°C for ∼20 min in the case of PA66 and at 200°C for ∼15 min in the case of POM. Plates of different thickness, in the range 3–12 mm, were produced for the present study.

Two samples of polyarylamide (PAR) containing 50 and 60 wt% glass fibres (G50 and G60) in the form of slit-gate injection moulded plates (125 × 125 mm) of nominal thickness 2 mm were supplied by Solvay, Brussels, Belgium.

2.2. Microstructural characterisation

The microstructure of all composite mouldings was characterised by determining fibre content (weight and volume fraction), fibre diameter, average fibre length and fibre length distribution, in the mass of each sample, and fibre orientation distribution through the thickness of the plates.

Fibre content and dimensions were regarded as uniform throughout the mouldings. They were measured on three pieces of material taken at random positions from each plate. To isolate the fibres from the polymeric matrix the latter was burned off in a muffle furnace at 700°C. From the residue weight and the known densities of glass and polymer, fibre weight and volume fraction were determined. The fibre aggregates were then immersed in acetone to ease their disentanglement. A sample containing at least 2000 fibres for each specimen was then examined under an optical microscope (Olympus BX60) equipped with image analysis facilities (videocamera and monitor JVC connected to an Apple LX II computer provided with the image analysis program Image 1.37) to measure fibre dimensions.

Fibre orientation was determined at six different in-plane positions of each plate. The method suggested by Advani and Tucker [11] was used. It consists of sectioning the plates and measuring the length of the axes of the elliptical cross-section of the fibres exposed on the section plane. To ease the microscopic observation the surface of the sections was polished using metallographic techniques, starting with rough polishing papers to end up with a 1 μm diamond polishing suspension. The quality of the appearance of the surface in the reflecting light microscope is determined by the different reflectance of the fibres and the matrix. In order to achieve sufficient contrast between fibres and matrix the polished (matrix) surface was etched with a diluted solution of formic acid.

To determine the fibre orientation distribution through the thickness B of the plate (at any in-plane position of the plate), a 1 mm wide strip was considered on the section surface and each strip was divided into 20 frames, each of which 1 mm wide and B/20 high

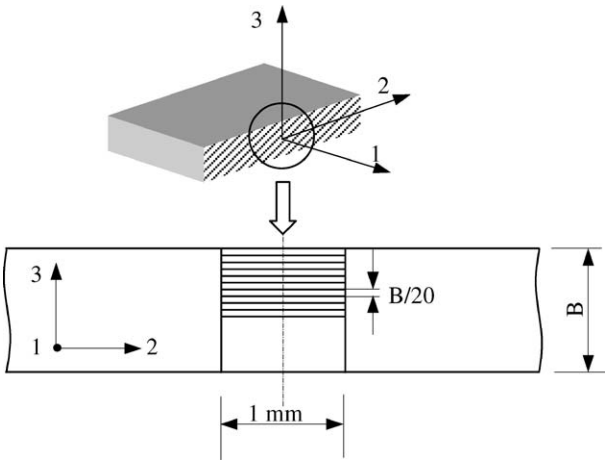

Figure 1 Specimen and observed section surface divided into 20 frames for fibre orientation distribution characterisation.

(Fig. 1). All the fibres (not less than 200) contained in each frame were considered to ensure unbiased determinations.

To measure the length of the axes of the elliptical cross-section of the fibres the same optical equipment mentioned above was used with an especially developed image analysis software [12].

The Advani-Tucker tensor used to describe fibre orientation is defined as:

$$a_{ij} = \frac{\sum_k \left(p_i p_j\right)_k l_k F_k}{\sum_k l_k F_k} \tag{1}$$

where p_i is the component with respect to axis i, of the unit vector $\vec{p}$ aligned with the k-th fibre (Fig. 2a), l_K is the fibre length and F_K a weighting factor required to convert a surface measurement into a volumetric property: it is related to the projection of the fibre length l_K on the normal n to the section plane (Fig. 2b) via the relationship:

$$F_k = \frac{1}{l_k \cos\theta_k} \tag{2}$$

which states that the probability for a sectioning plane of cutting a fibre is proportional to the projection of the fibre length onto the normal to the section plane.

To study the influence of fibre orientation on stress-strain and fracture behaviour, fibre orientation must be considered in relation to the applied stress direction. It was expected that the orientation factor in the applied stress direction would show the most evident relationship with the considered mechanical properties. The orientation tensor components $[a^0]$ were thus measured on just one plane and then transformed into the required orientation factors $[a]$ with respect to the applied stress direction. The section plane, on which the measurements were taken, was the one normal to the plate and to the extruded rods direction or to the mould fill direction (plane 2–3° in Fig. 3a). The components $[a]$ defined with respect to a reference axis system rotated "in plane" by an angle α were obtained from the components a^0_{ij} of the primitive orientation tensor $[a^0]$ via conventional matrix algebra.

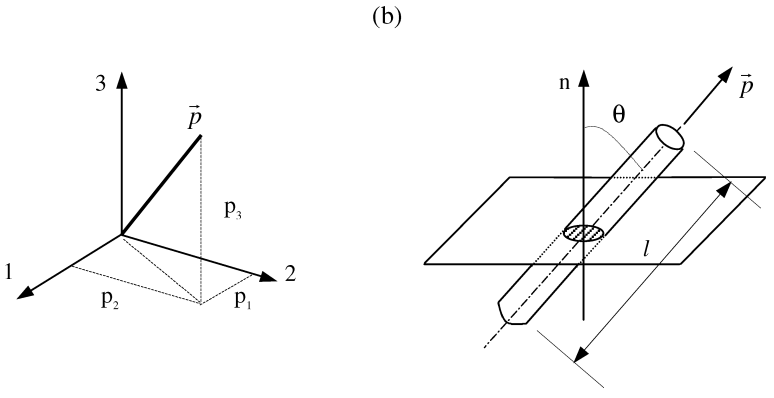

Figure 2 (a) Unit vector $\vec{p}$ and (b) fibre length projection.

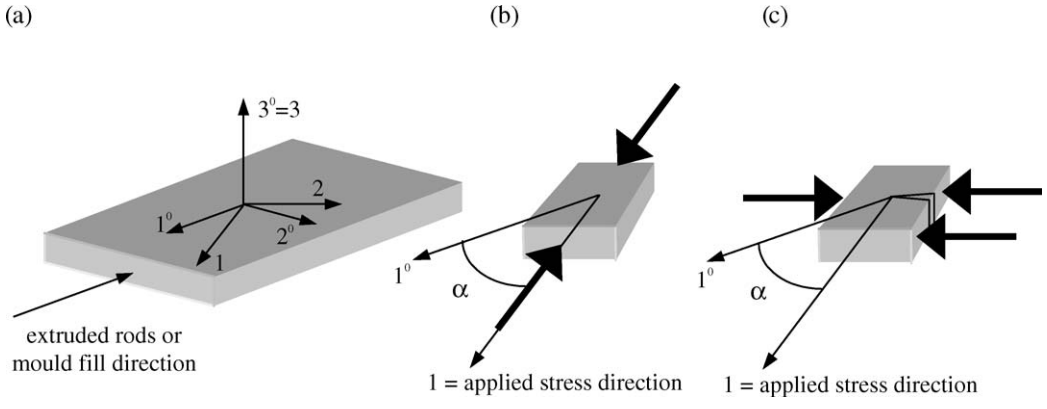

Figure 3 Reference systems and (a) material plate; (b) uniaxial tension or compression specimen; (c) fracture specimen.

2.3. Mechanical testing

Uniaxial tension and uniaxial compression tests were carried out on specimens cut from the unidirectional materials plates at varying angles α between the intended direction of the stress to be applied and the extruded rods or mould fill direction (Fig. 3b). "Dog-bone" specimens for tension tests were machined according to ISO 527-2 [13], whereas prismatic specimens with a square base of side B (the plate thickness) and height $H = 1.5B$ were used in compression tests according to ISO 604 [14] with sheets of Teflon inserted between the specimen and the machine plates to reduce friction. A strain rate of 0.01 s^{-1} was used in all tests. Young's modulus and yield stress values were sought from the stress-strain curves. The yield point was identified with either a maximum or a knee in the stress-strain curve.

Mode I fracture tests were performed in three-point bending according to ESIS testing protocol (now an ISO standard [15]) at a crosshead speed of 10 mm·min^{-1}. Fracture specimens were cut at varying angles α between the direction perpendicular to the notch plane (the "applied stress" direction) and the extruded rods or mould fill direction (see Fig. 3c). Specimen dimensions were: width $W = 3B$, span $S = 4W$, initial notch depth $a_0 = 0.5W$ and specimen thickness B was the plate thickness. Notches were made by sliding a truncated razor blade, scalpel wise. The notch root radius was ∼13 μm. Fracture toughness was determined at fracture initiation and that point was identified from the load diagram. The critical stress intensity factor K_C and fracture energy G_C were determined independently from the load and the energy at fracture initiation, respectively, as stated in the standard. Linearity requirements set out in the standard were generally satisfied.

All specimens were kiln dried at 80°C for 16 h just before testing. All mechanical tests were carried out a 23°C on an Instron 1125 testing machine computer controlled.

2.4. Fractography

After fracture, the fracture surface was observed under a scanning electron microscope (SEM) to assess the fracture mechanisms involved.

3. Results and discussion

3.1. Microstructure

Average fibre content (weight and vol%) and dimensions (diameter and number and mass average length) are given in Table I for the different materials

TABLE I Average fibre content and dimensional characteristics

Material	w_f (%)	v_f (%)	l_n (μm)	l_m (μm)	d_m (μm)
Polyamide 6.6 G30 A	28.8	15.4	417	544	11
Polyamide 6.6 G30 B	28.6	15.3	420	551	11
Polyoxymethylene G15	14.9	8.8	144	197	12
Polyoxymethylene G30	29.9	19.1	122	172	12
Polyarylamide G50	50.6	32.7	134	186	9
Polyarylamide G60	60.7	42.3	127	172	9

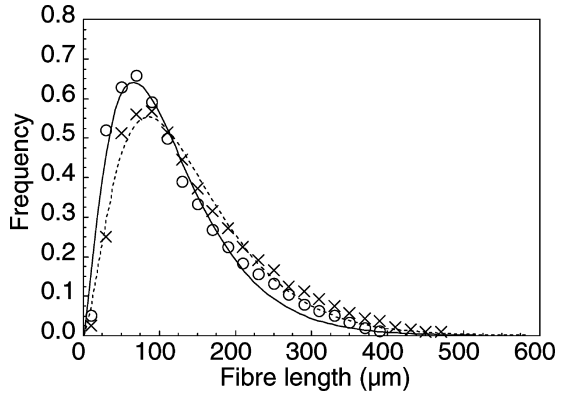

Figure 4 Fibre length distribution: polyoxymethylene G15 (-×-) and G30 (-○-).

investigated. No difference was noted at different positions of the same plate. Differences in fibre length (mean and distribution) between samples of the same polymer reinforced with different fibre contents reflect the fibre degradation occurring during processing: fibre breaking occurring in the course of the extrusion and injection moulding processes affects more extensively the material with a higher fibre content. Fig. 4 shows the case of the two reinforced polyoxymethylenes as an example. All the materials studied in the present work showed a fibre length distribution of the Weibull type [16].

Fibre orientation represented the major difference between different mouldings. In PA 6.6 G30, A and B, and in POM, G15 and G30, prepared by hot compression of thin extruded rods, fibre orientation turned out to be indeed highly unidirectional ($a_1^0 \approx 1$, $a_{22}^0 = a_{33}^0 \approx 0$) and uniform through the thickness B. In PAR, G50 and G60, plates of 2 mm thickness, obtained by slit-gate injection moulding, fibre orientation varies somewhat through the thickness B. In the two outer layers the fibres are substantially aligned with the mould fill direction ($a_1^0 \approx 1, a_{22}^0 = a_{33}^0 \approx 0$), whereas at the midplane there is a "core" layer in which the fibres are disoriented although laying in the plane ($a_1^0 = a_{22}^0 \approx 0.6$, $a_{33}^0 \approx 0$). In view of the very thin thickness of this "core" layer also the plates of polyarylamide were considered as nominally unidirectional for the purpose of the present study. Fig. 5 shows a comparison between through-thickness fibre orientation distributions in PA 6.6 G30 A and PAR G50. It is worth noting that a value of a_{33}^0 close to zero was generally obtained, i.e., fibre orientation is in any case substantially planar.

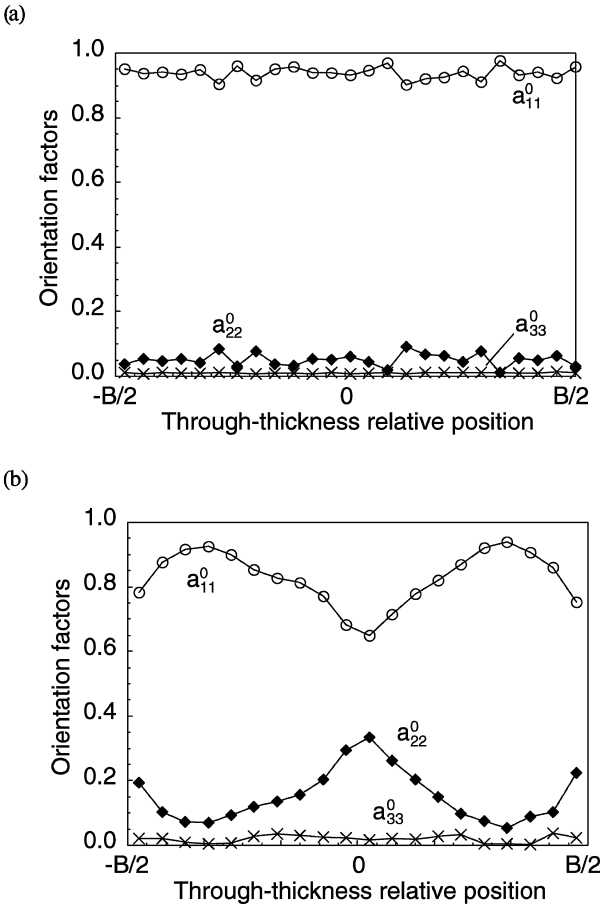

Figure 5 Fibre orientation factors a_{ii}^0: (a) polyamide 6.6 G30 A and (b) polyarylamide G50.

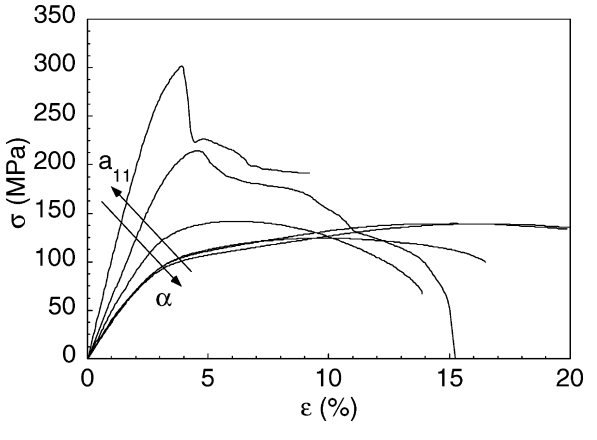

Figure 6 Stress-strain curves recorded in uniaxial compression tests on polyamide 6.6 G30 A specimens cut at varying angle α.

3.2. Stress-strain behaviour

Stress-strain traces recorded in uniaxial tension and uniaxial compression tests performed on specimens cut at different angles α between the applied stress direction and the (nominal) fibre direction showed quite different shapes with varying angles α. An increase in fibre alignment with respect to the direction of the applied stress (i.e., decrease in α, increase in a_{11}) constantly involves an increase in stiffness and strength, a reduction up to full suppression of cold drawing and subsequent strain hardening, and a decrease in ultimate strain. Fig. 6 shows the stress-strain curves recorded in uniaxial compression tests performed on PA 6.6 G30 A as an example. The initial section of the stress-strain curves appears to be very influenced by fibre orientation, but only for angles α less than 45° ($a_{11} > 0.5$). At lower orientation factor values both material stiffness and compressive strength become almost independent of fibre orientation.

Young's moduli determined from the slope of the initial linear part of the stress-strain curves are reported as a function of the fibre orientation factor a_{11} in Fig. 7.

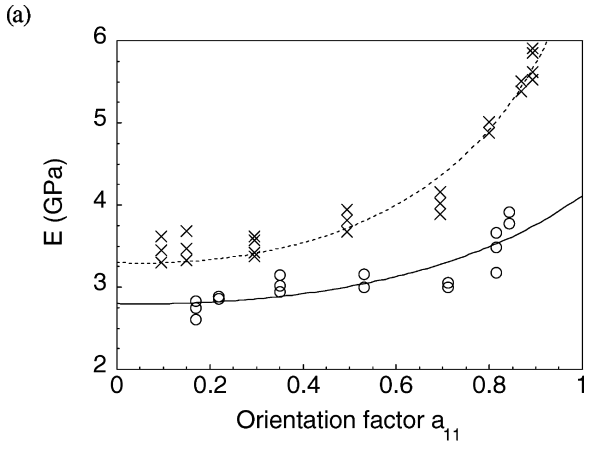

Polyoxymethylene G15: $E_{11} = 4.1$ GPa, $E_{22} = 2.8$ GPa, $G_{12} = 1.2$ GPa, $\nu_{12} = 0.28$
Polyoxymethylene G30: $E_{11} = 7.0$ GPa, $E_{22} = 3.3$ GPa, $G_{12} = 1.4$ GPa, $\nu_{12} = 0.25$

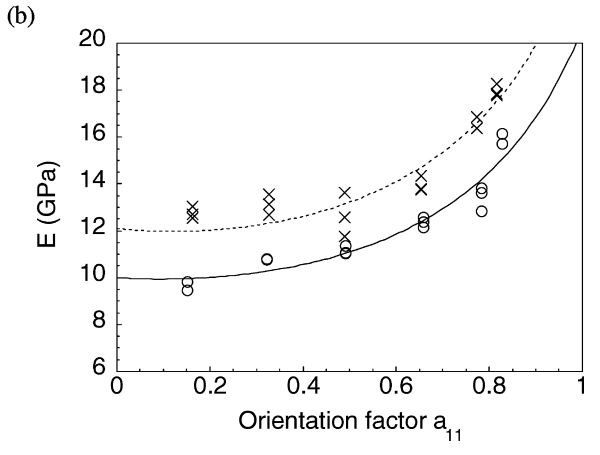

Polyarylamide G50: $E_{11} = 20.6$ GPa, $E_{22} = 10.0$ GPa, $G_{12} = 4.3$ GPa, $\nu_{12} = 0.20$
Polyarylamide G60: $E_{11} = 24.3$ GPa, $E_{22} = 12.1$ GPa, $G_{12} = 5.1$ GPa, $\nu_{12} = 0.20$

Figure 7 Young's modulus E versus fibre orientation factor a_{11}: (a) polyoxymethylene G15 (-○-) and G30 (-×-), (b) polyarylamide G50 (-○-) and G60 (-×-). Points: experimental; lines: best fitting to Equation 3. Reported values of the parameters E_{11}, E_{22}, G_{12} and ν_{12} are best fitting values.

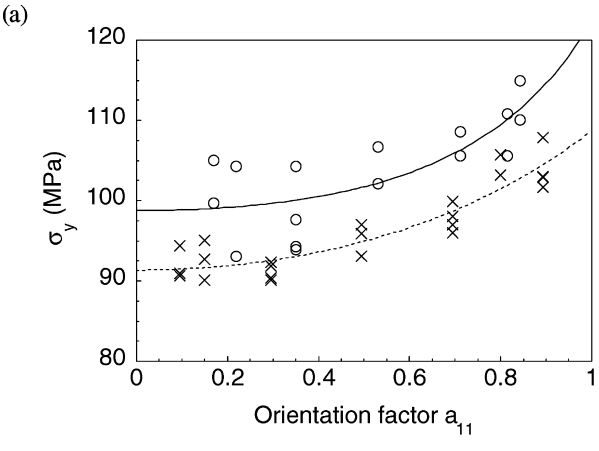

Polyoxymethylene G15: $\sigma_1^u = 108.8$ MPa, $\sigma_{22}^u = 91.3$ MPa, $\tau_{12}^u = 70.0$ MPa
Polyoxymethylene G30: $\sigma_1^u = 122.3$ MPa, $\sigma_{22}^u = 98.8$ MPa, $\tau_{12}^u = 73.4$ MPa

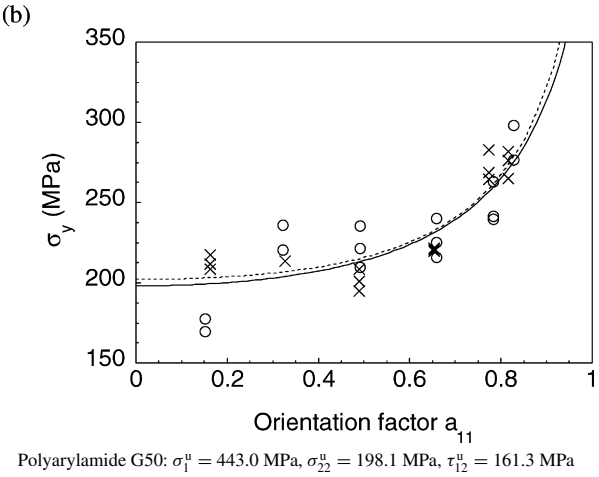

Polyarylamide G50: $\sigma_1^u = 443.0$ MPa, $\sigma_{22}^u = 198.1$ MPa, $\tau_{12}^u = 161.3$ MPa
Polyarylamide G60: $\sigma_1^u = 500.0$ MPa, $\sigma_{22}^u = 202.2$ MPa, $\tau_{12}^u = 158.5$ MPa

Figure 8 Yield stress σ_y versus fibre orientation factor a_{11}: (a) polyoxymethylene G15 (-○-) and G30 (-×-); (b) polyarylamide G50 (-○-) and G60 (-×-). Points: experimental; lines: best fitting to Equation 4. Reported values of the parameters σ_1^u, σ_{22}^u e τ_{12}^u are best fitting values.

No significant difference was found between the two samples of PA 6.6 G30, *A* and *B*, having different fibre surface treatments (not shown), whereas an increase in fibre content causes an increase in Young's modulus in both reinforced POM (Fig. 7a) and PAR (Fig. 7b).

For all materials studied in this work the experimental data can be well fitted by the equation that was formulated to describe the Young's modulus in continuous unidirectional fibre composite [1]:

$$E(a_{11}) = \left[\frac{(a_{11})^2}{E_{11}} + \frac{(1-a_{11})^2}{E_{22}} + \left(\frac{1}{G_{12}} - \frac{2\nu_{12}}{E_{11}}\right) \cdot a_{11} \cdot (1-a_{11})\right]^{-1} \quad (3)$$

in which E_{11}, E_{22}, G_{12} e ν_{12} are the elastic properties (Young's modulus, shear modulus and Poisson's ratio) in the principal directions (where *1* is the nominal fibre direction).

This equation appears then to be applicable to both continuous and discontinuous unidirectional fibre composites at varying angle between the applied stress direction and the fibre direction.

Yield stress values obtained from the same tests are plotted as a function of the fibre orientation factor a_{11} in Fig. 8. These experimental data can be well fitted by the equation proposed by Tsai-Hill for continuous fibre composites [1]:

$$\sigma^u = \left[\frac{(a_{11})^2}{\left(\sigma_{11}^u\right)^2} - \frac{(a_{11})^2 \cdot [1-(a_{11})^2]}{\left(\sigma_{11}^u\right)^2} + \frac{[1-(a_{11})^2]^2}{\left(\sigma_{22}^u\right)^2} + \frac{(a_{11})^2 \cdot [1-(a_{11})^2]}{(\tau_{12}^u)^2}\right]^{-1/2} \quad (4)$$

where σ_{11}^u, σ_{22}^u e τ_{12}^u are the failure stresses.

Also in this case no significant difference was found between the two samples of PA 6.6 G30, *A* and *B*. By contrast, the two different matrixes, POM and PAR, show a different trend in the dependence of the yield stress of their composites on fibre content: when the fibre content increases the yield stress increases very slightly in PAR, whereas it decreases in POM.

3.3. Fracture toughness

Also the loading curves recorded in fracture tests exhibited quite a different shape with varying fibre

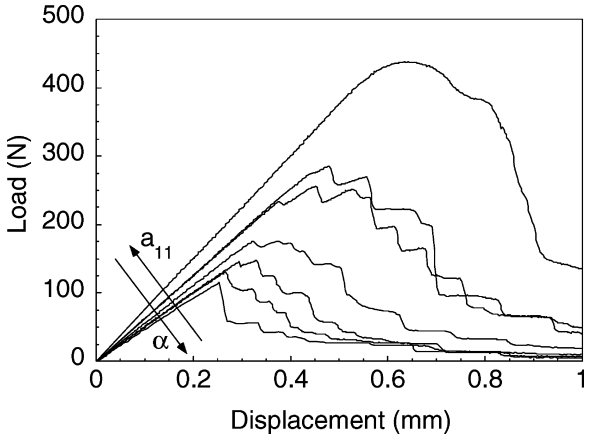

Figure 9 Loading curves recorded in fracture tests on polyamide 6.6 G30 A specimens cut at varying angle α.

orientation angle α: Fig. 9 shows an example. In particular, the degree of non-linearity observed prior to the attainment of the maximum load decreases as the angle α increases. In general, the peak becomes sharper and unstable fracture occurs earlier as α increases. Non-linearity can be mainly attributed to the mechanism of fibre pull-out in these materials while unstable fracture can rather be associated with fibre debonding.

It is worth noting that the loading curves recorded with reinforced PA 6.6 and PAR in the α range $30^\circ < \alpha < 60^\circ$, are not monotonic before the maximum, i.e., a sort of "pop-in" occurs: fracture starts and the crack grows to some extent (see the load drop, i.e., increase in compliance) before it arrests and the load resumes increasing. A series of "slip-stick" events may follow, producing a V-teeth-saw-shaped trace in the loading curve. In these cases it is observed that the direction of the crack soon deviates from the plane of the original notch to bend toward the prevailing direction of the fibres. This deviation from symmetry may explain the discontinuous crack propagation. As a matter of fact with reinforced POM crack propagation almost doesn't deviate from the original notch plane and "pop-in" or slip-stick behaviour is not observed. Whatever the shape of the loading curve, the point of fracture initiation was identified following the rules set out in [15].

According to Friedrich [4] and Friedrich *et al.* [5, 6] the fracture toughness of short fibre composites can be described in term of a parameter, called reinforcing effectiveness, R, which compounds several microstructural characteristics: the fibre volume fraction v_f, the fibre aspect ratio l_n/d, the width of the fibre length distribution l_n/l_m, and the average fibre orientation over the fractured cross-section. This last one is expressed by the above authors by means of an "effective fibre orientation parameter," $f_{p,eff}$, arbitrarily defined in order to consider the crack hindrance effects of the fibres due to their local orientation. The parameter R is then expounded as the product of the above characteristics, as follows:

$$R = v_F\left(\frac{l_n}{d}\right)\cdot\left(\frac{l_n}{l_m}\right)f_{p,eff} \qquad (5)$$

and the critical stress intensity factor K_C is claimed to bear a linear relationship with R, the slope of which depends on the energy dissipation mechanisms occurring at fracture.

At variance with Friedrich [4] and Friedrich *et al.* [5, 6] assumptions the critical stress intensity factor K_C and fracture energy G_C, measured at fracture initiation in the present work are reported as a function of the fibre orientation factor a_{11}, as shown in Figs 10, 11, 12a and b. All the systems examined show the same fundamental result found by Lumini and Pavan previously [7]: the plot of K_C versus a_{11} shows a bi-linear relationship, with different slopes over different ranges of the orientation factor and a sharp "knee" between the two linear branches at a "critical" value of the orientation factor, $(a_{11})_C$. The same type of relationship is found for G_C.

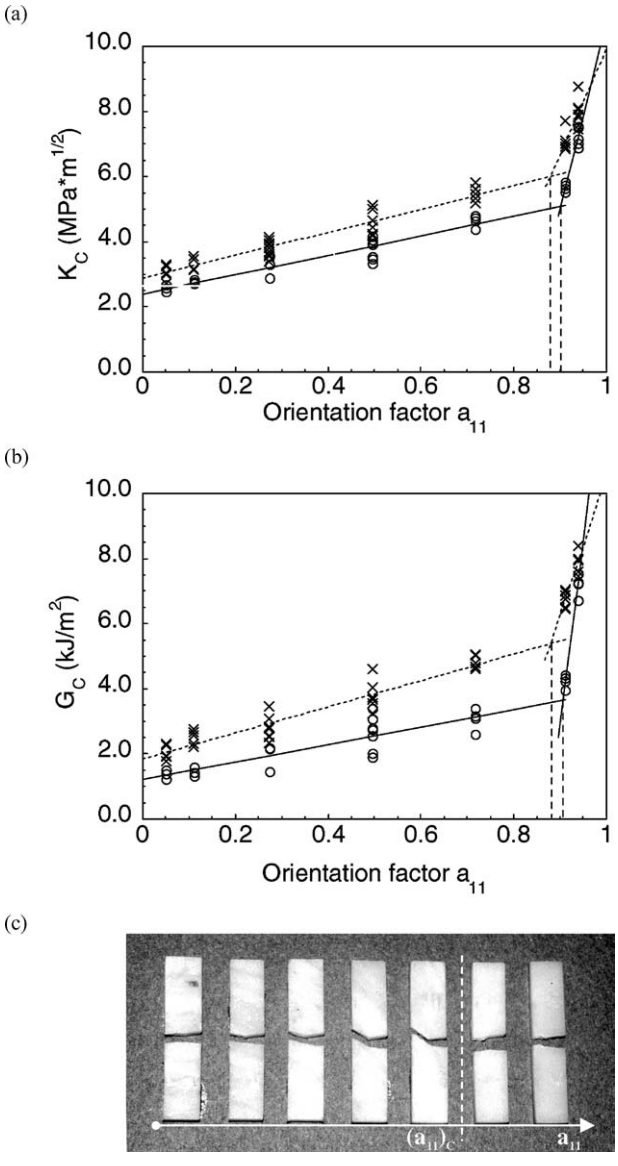

Figure 10 (a) Critical stress intensity factor K_C versus fibre orientation factor a_{11}: polyamide 6.6 G30 A (-○-) and B (-×-); (b) Critical fracture energy G_C versus fibre orientation factor a_{11}: polyamide 6.6 G30 A (-○-) and B (-×-); (c) Lateral view of the two broken halves of polyamide 6.6 G30 A specimens showing deviation of the crack (on the left side of the specimen) from the notch plane (on the right side of each specimen) for varying a_{11} (see arrow).

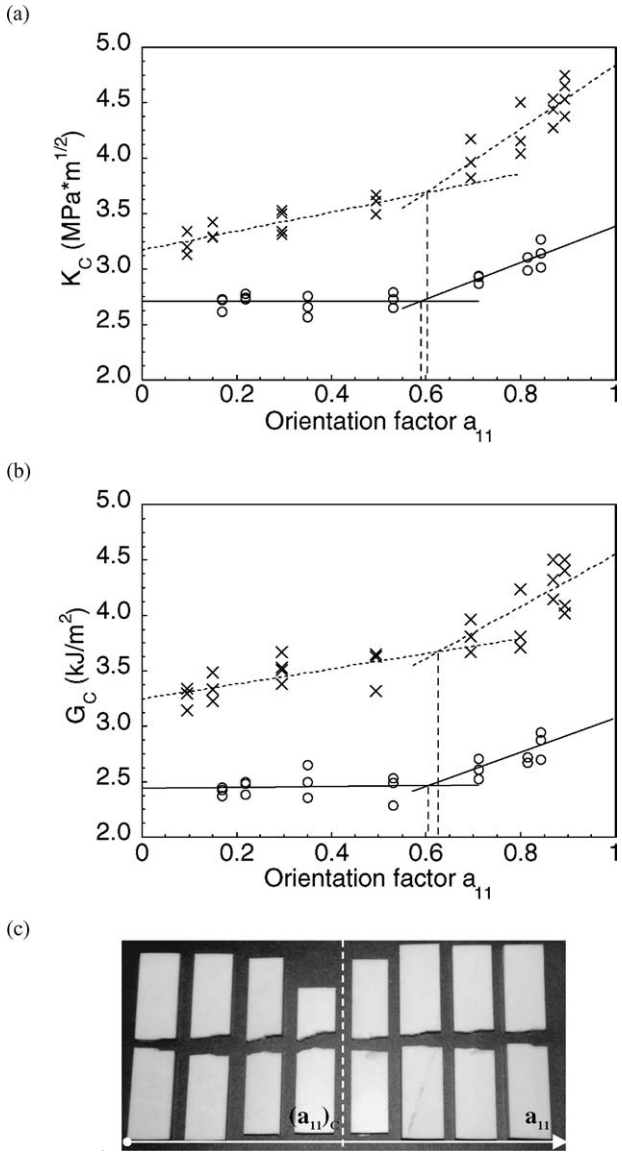

Figure 11 (a) Critical stress intensity factor K_C versus fibre orientation factor a_{11} polyoxymethylene G15 (-○-) and G30 (-×-); (b) Critical fracture energy G_C versus fibre orientation factor a_{11}: polyoxymethylene G15 (-○-) and G30 (-×-); (c) Lateral view of the two broken halves of polyoxymethylene G30 specimens showing deviation of the crack (on the left side of the specimen) from the notch plane (on the right side of each specimen) for varying a_{11} (see arrow).

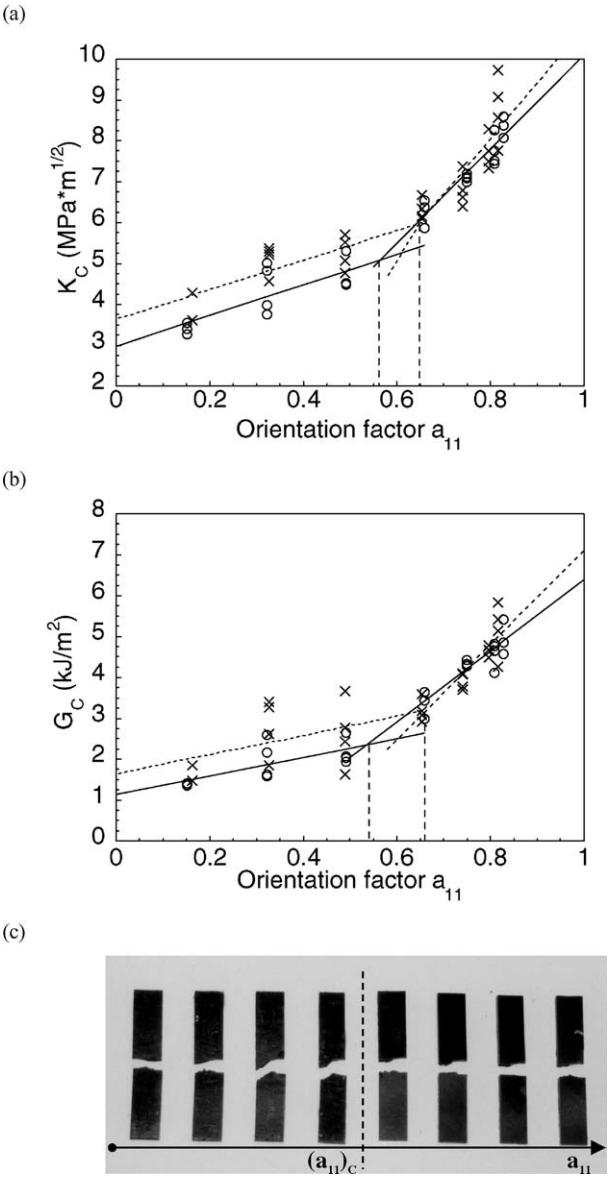

Figure 12 (a) Critical stress intensity factor K_C versus fibre orientation factor a_{11} polyarylamide G50 (-○-) and G60 (-×-); (b) Critical fracture energy G_C versus fibre orientation factor a_{11}: polyarylamide G50 (-○-) and G60 (-×-); (c) Lateral view of the two broken halves of polyarylamide G50 specimens showing deviation of the crack (on the left side of the specimen) from the notch plane (on the right side of each specimen) for varying a_{11} (see arrow).

The existence of that "knee" is corroborated by the observation of the crack growth direction. The crack proceeds in the notch plane direction in specimens with $a_{11} > (a_{11})_C$, whereas soon deviates from the plane of the original notch to follow the prevailing direction of the fibres when $a_{11} < (a_{11})_C$, as shown in Figs 10c, 11c, and 12c.

The sharp variation in toughness and the sudden change in crack growth direction at $(a_{11})_C$ can be interpreted as a transition between different fracture mechanisms. This interpretation is supported by the scanning electron microscopic analysis of the fracture surfaces. Test specimens with $a_{11} < (a_{11})_C$ showed a smooth fracture surface displaying clean looking fibres. Test specimens with $a_{11} > (a_{11})_C$ showed a rough fracture surface where fibre pulled-out and voids left behind by pulled-out fibres are evident. Thus, on increasing orientation factor the failure mechanism changes from fibre debonding (and matrix fracture) to fibre pull-out. Fig. 13a and b show an example of fracture surfaces of POM G30 at a low and a high orientation factor respectively.

In the microscopic analysis of the fracture surfaces, fibre breakage was never observed in any of the materials examined. This can be explained as due to the fact that the fibres were too short. Indeed, it is well known that a critical fibre length, l_C, exists which separates two different fracture mechanisms. Fibre pull-out is the prevailing fracture mechanism when fibre length is smaller than the critical fibre length ($l < l_C$), whereas fibre breakage occurs when fibre length is larger than the critical one ($l > l_C$). The critical fibre length is calculated used the relationship [1]:

$$l_C = \frac{\sigma_f^*}{2\tau_i^*} d \tag{6}$$

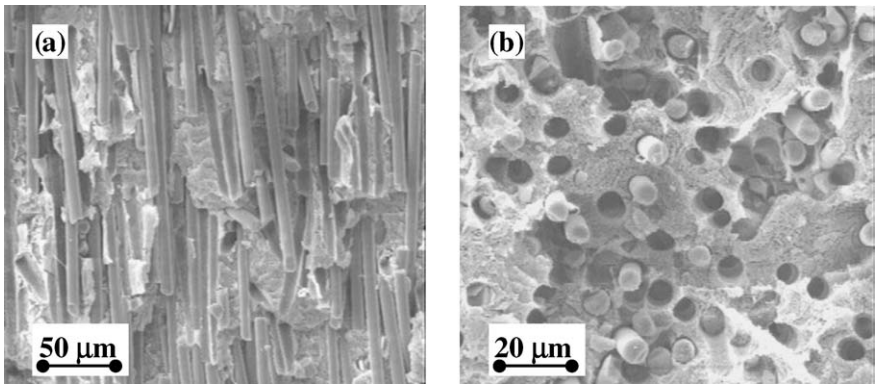

Figure 13 Scanning electron micrographs of fracture surfaces of polyoxymethylene G30 (a) at low orientation factor, $a_{11} \sim 0$ and (b) at high orientation factor, $a_{11} \sim 1$.

where σ_f^* is the tensile strength of the fibres, τ_i^* is the shear strength of the fibre-matrix adhesion and d is the fibre diameter. Assuming $\sigma_f^* = 3$ GPa and $\tau_i^* = 10$ MPa as typical values for our materials and taking the values of fibre diameters reported in Table I, the estimated critical fibre lengths turn out to be $l_C \sim 1650$, 1800 and 1350 μm for polyamide 6.6, polyoxymethylene and polyarylamide respectively: i.e., in any case larger than the measured average fibre length (Table I).

From the results of Figs 10–12 it appears that the slopes of the two linear sections of the K_C vs. a_{11} and G_C vs. a_{11} plots and the critical value of the fibre orientation factor, $(a_{11})_C$, vary from system to system, i.e., they may depend on all the internal variables considered in this work. The data gathered in the present work, although vast, are not enough even to attempt to find a correlation between the properties observed (slopes of K_C vs. a_{11} or G_C vs. a_{11} and critical value of the fibre orientation factor, $(a_{11})_C$) and the single internal variables examined. It can only be surmised that, just as the critical fibre length (see Equation 6) they may depend on the internal variables via the fibre tensile strength, the fibre-matrix interface shear strength (which depends also on the fibre surface treatment) and fibre dimensions.

It is worth asking why previous authors did not find a distinct "knee" in the thoughness-vs-orientation dependence. We can think of two possible reasons. First, to the best of our knowledge well aligned unidirectional samples were never examined previously; second, the use of an "effective fibre orientation parameter" having a smooth dependence on fibre orientation such as that assumed by Friedrich [4] and Friedrich *et al.* [5, 6] would anyway mask any sharp transition effect between different fracture mechanisms.

4. Conclusions

In the present work the dependence of fracture toughness on fibre orientation was investigated in a wide range of unidirectional short fibre composites by varying several internal variables. All systems examined present a distinct discontinuity in the K_C vs. a_{11} and G_C vs. a_{11} plots for a certain fibre angle, which is interpretable as a transition between different fracture mechanisms involved with varying fibre orientation. This interpretation is supported by the observation of the crack growth direction and the analysis of the fracture surfaces. Matrix fracture and fibre debonding are the prevailing fracture mechanisms at low values of the fibre orientation factor, while at high values of the fibre orientation factor fibre breakage or pull-out, depending on fibre length, is the main fracture mechanism. This implies that a "critical" fibre angle should also be considered in addition to a critical fibre length in order to evaluate fracture toughness in materials having a complex microstructure such as those obtained by injection moulding.

Acknowledgements

This work is part of the PhD thesis sustained by S. F. at Politecnico di Milano. Part of the results reported in this paper were presented previously at "EUROMAT 2000: Conference on Advances in Mechanical Behaviour, Plasticity and Damage," Tours (France), November 2000, and at the "6th International Conference: Deformation and Fracture of Composites," Manchester (UK), April 2001.

The authors would like to thank Radici NovaCips SpA, Villa D'Ogna (Italy), Rhodia Srl, Ceriano Laghetto (Italy) and Solvay SA, Brussels (Belgium), for kindly supplying the glass fibre reinforced samples of polyamide 6.6, polyoxymethylene and polyarylamide respectively.

References

1. A. KELLY and N. H. MACMILLAN, "Strong Solids" (Clarendon Press, Oxford, 1986).
2. S. HASHEMI and J. MUGAN, *J. Mater. Sci.* **28** (1993) 3983.
3. D. D. HUANG, *Polym. Compos.* **16** (1995) 10.
4. K. FRIEDRICH, *Compos. Sci. Technol.* **22** (1985) 43.
5. J. KARGER-KOCSIS and K. FRIEDRICH, *ibid.* **32** (1988) 293.
6. J. KARGER-KOCSIS, R. WALTER and K. FRIEDRICH, *J. Polym. Eng.* **8** (1989) 221.
7. F. LUMINI and A. PAVAN, *Plast. Rubber Compos. Process. Appl.* **27** (1998) 240.
8. N. S. CHOI and K. TAKAHASHI, *J. Mater. Sci.* **31** (1996) 731.
9. F. LAPIQUE, R. H. GAARDER and A. LARSEN, *J. Reinf. Plast. Compos.* **20** (2001) 744.
10. S. FARA and A. PAVAN, in "Fracture of Polymers, Composites and Adhesives II," edited by J. G. Williams and A. Pavan (ESIS Publ., Elsevier, in press).

11. S. G. ADVANI and C. L. TUCKER, *J. Rheol.* **31** (1987) 751.
12. M. PICCARDI, Software for Image Analysis Especially Developed for the Present Work.
13. International Standard ISO 527-2 "Plastics—Determination of Tensile Properties—Part 2: Test Conditions for Moulding and Extrusion Plastics" (1993).
14. International Standard ISO 604 "Plastics—Determination of Compressive Properties" (2002).
15. International Standard ISO 13586 "Plastics—Determination of Fracture Toughness G_{IC} and K_{IC}—Linear Elastic Fracture Mechanics (LEFM) Approach," 1st edn., 2000.
16. W. WEIBULL, *J. Appl. Mech.* **18** (1951) 293.

Received 11 July 2003
and accepted 5 February 2004